18th International Conference on Information Fusion
Washington, DC - July 6-9, 2015

Target Detection Using GPS Signals of Opportunity

Maria-Paola Clarizia
Atmospheric, Oceanic and Space Sciences
University of Michigan
Ann Arbor, U.S.A.
clarizia@umich.edu

Christopher S. Ruf
Atmospheric, Oceanic and Space Sciences
University of Michigan
Ann Arbor, U.S.A.
cruf@umich.edu

Paolo Braca
NATO Science & Technology Organization
Centre for Maritime Research and Experimentation
La Spezia, Italy
Paolo.Braca@cmre.nato.int

Peter Willett
Electrical and Computer Engineering
University of Connecticut
Storrs, U.S.A.
willett@engr.uconn.edu

Abstract – ***We investigate the capability of GPS signals of opportunity to detect and localize targets on the sea surface. The proposed approach to target detection is new, and stems from the advantages offered by GPS-Reflectometry (GPS-R) in terms of spatial and temporal sampling, and low cost/low power technology, extending the range of applications of GPS-R beyond remote sensing. Here the exploitation of GPS signals backscattered from a target is proposed, to enhance the target return with respect to the sea clutter. A link budget is presented, showing that the target return is stronger than the background sea clutter when certain conditions are verified. The findings agree with the only empirical measurement found in literature, where a strong return from a target was fortuitously registered during an airborne campaign. This study provides a first proof-of-concept of GPS-based target detection, highlighting all the potentials of this innovative approach.***

Keywords: GPS, detection, backscattering, target, surface vessel, link budget.

1 Introduction

Global Navigation Satellite System-Reflectometry (GNSS-R) uses signals of opportunity from navigation constellations (e.g. GPS, GLONASS and Galileo), reflected off the surface of the ocean, to retrieve geophysical parameters such as ocean surface wind speed, sea state, and sea surface height (see figure 1a) [1]-[3]. GNSS-R is primarily employed for scatterometric applications, focusing on the retrieval of wind speed, and it is based on a bistatic configuration, where transmitters and receivers are located on different platforms. The signal that reaches the receiver is in a forward scattering configuration and is mainly reflected by a specular point on the surface and an area around the specular point called glistening zone (see Figure 1b). The size of the glistening zone typically depends on the roughness of the sea surface, which is related to wind speed. The GNSS-R receivers exploit the delay and Doppler information in the reflected GPS signals to generate 2D maps of scattered power as a function of delay and Doppler frequency, known as Delay–Doppler Maps (DDMs). An example of DDM acquired during the GNSS-R experiment onboard the UK- DMC Satellite, in 2005 [4-5], is shown in Figure 2. The delay refers to the time it takes for the signal to travel from the transmitter to the sea surface, and from the sea surface to the receiver. Delays are usually expressed in units of chips, where 1 chip is about 1 μs and represents the duration of the single rectangular pulse of the GPS Coarse/Acquisition (C/A) code [6]. The Doppler frequency shift is the shift in the frequency of the signal caused by the relative motion of transmitter and receiver. Each DDM pixel is obtained through a cross-correlation of the received scattered GPS signal with a locally generated replica of the C/A code of the transmitted signal, shifted in delay and Doppler by the values of the DDM pixel itself. Such coherent cross-correlation is usually performed over 1 ms [4-5], and hence is heavily affected by speckle noise, so that a number of incoherent accumulations of consecutive cross-correlation values is also necessary to reduce the speckle. A typical incoherent accumulation time for DDM measured spaceborne is 1 second. The DDM peak represents the power scattered from the specular point, whereas the remaining power forms a horseshoe-like shape in the DDM that represents the power scattered from the glistening zone. The shape and amplitude of the DDMs are related to wind speed and are usually exploited to infer the wind information.

GNSS-R is considered an innovative and advantageous remote sensing technique. Its main advantages lie in the exploitation of pre-existing transmitters, the global coverage and high space-time sampling that can be achieved through the use of all the scattered navigation signals, and the use of simple receivers to implement such technique. The receivers commonly employed in GNSS are modified standard GNSS receivers. As such, they are

(a)

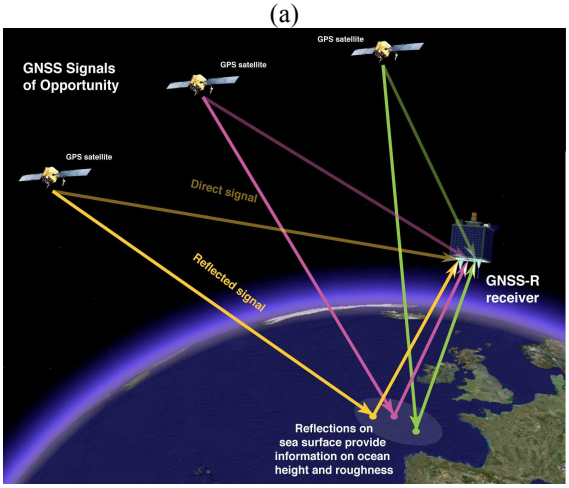

(b)

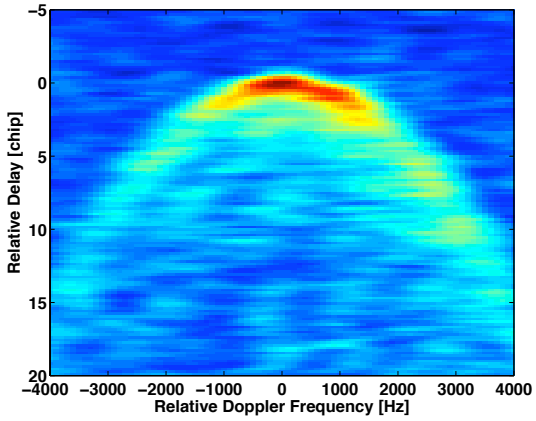

Figure 1. (a) illustration of how GNSS-R works for bistatic scatterometry and altimetry. The direct signals from the GPS satellites to the receiver are used as reference (i.e. to locate the reflection point on the surface) while the reflected GPS signals carry information on the sea surface roughness, related to wind speed, or on sea surface height. (b) example of Delay-Doppler Map (DDM), which represents scattered GPS power as a function of delay and Doppler frequency. The delays are expressed in GPS Coarse/Acquisition (C/A) code chips, where 1 chip is about 1 μs.

cheap, low-power and light-weight, and accommodated on a variety of platforms. These properties of reflected navigation signals, coupled with the capability of the L-Band GPS signals to penetrate through heavy rain, have led to the recent selection of the NASA Earth Venture spaceborne Cyclone Global Navigation Satellite System (CYGNSS) mission, a constellation of 8 microsatellites in Low-Earth Orbit (LEO) with equatorial inclination, which will retrieve wind speed in Tropical Cyclone (TC) conditions, particularly in the TC inner core, using the GPS-R technique [7-8]. The coverage expected from CYGNSS over a period of 24 hours represents a nearly gap-free observation of the latitudinal band where most of the TCs occur, and it is currently not achievable by any other existing satellite.

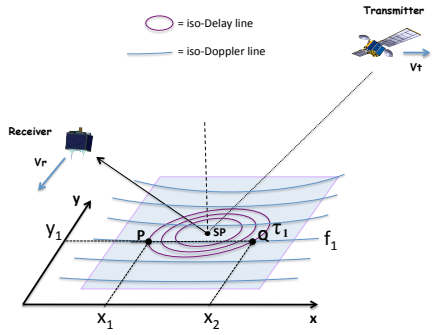

Figure 2. Illustration of iso-delay (ellipses) and iso-Doppler (parabolae) lines for bistatic geometry and a forward scattering configuration [14]. The intersection of the iso-delay ellipse at delay τ_1 and the iso-Doppler parabola at Doppler f_1 corresponds to two points in space (P and Q).

2 Use of GPS-Reflectometry for Sea Surface Target Detection

A new application that has recently arisen is to use GNSS signals of opportunity for target detection and localization. The capability of target detection using GPS-R has thus far only been investigated in a handful of studies [9-13]. The existing studies all focus on the exploitation of GPS-R in a forward scattering configuration, which is the configuration traditionally adopted for remote sensing, as shown in Figure 1a. The forward scattering configuration generates a number of issues for target detection, which can be summarized as follows:

1) The reflection from the specular point remains the predominant one in DDMs, whereas potential reflections from targets manifest themselves as secondary peaks in the DDMs [9]. It is often very difficult to separate the secondary peaks that come from targets from speckle noise affecting DDMs.
2) The technique works better for static or slow-moving receiver platforms. Indeed, the number of secondary reflections decreases rapidly with increasing averaging time [10]. The weaker secondary reflections from the target are rapidly attenuated because the scattered power becomes incoherent as the receiver moves and the receiver viewing geometry changes.
3) The target geolocation is ambiguous. This is due to the fact that a given Delay Doppler (DD) pixel in the DDM corresponds in space to the intersection of a locus of constant delay values, called iso-delay line, with a locus of constant Doppler frequency shift, called iso-Doppler lines. Iso-delay lines usually have the form of quasi-concentric ellipses, while iso-Doppler lines are shaped as parabolae (Figure 2, from [14]). Thus,

with the exception of the specular point itself, these lines intersect each other in two points, such that a DD pixel corresponds to two distinct points in space [15].

The issues listed above suggest that a backscattering configuration is a measurement geometry preferable to the forward scattering configuration. In a backscattered mode, when the receiver is more or less in line between the GPS satellite and the target (i.e. the aspect angle defined by transmitter, target and receiver is not too large), the targets can exhibit an enhanced "corner reflector" effect that focuses scattered power back toward the source. In addition, the background clutter due to scattering from the ocean surface is considerably lower (by ~20 dB relative to the forward scatter geometry at typical surface wind speeds). An illustration of the backscattering configuration for the target detection application is shown in figure 3. Note the difference with respect to the forward scattering configuration, shown in Figure 1a. In the backscattering case, the direct signals provide a reference for transmitter and receiver positions, and the backscattered signals provide information on presence and position of the target on the sea surface.

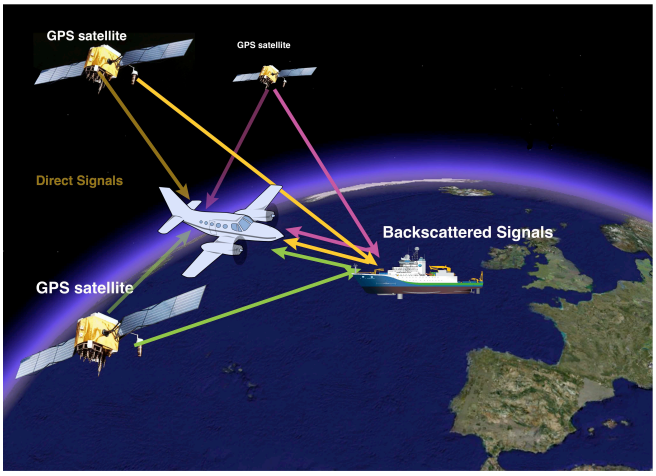

Figure 3. GPS-Reflectometry in a backscattering configuration, for detecting targets on the sea surface.

Some of the intuitive advantages of such configuration for the target detection application are therefore: 1) a much stronger backscattering from the target, whenever a corner reflector geometry is present in the target; 2) weaker sea clutter, due to the fact that the backscattered L-band GPS signal from the sea surface is very weak; and 3) The elimination of spatial ambiguities that exist in the forward scattering configuration, thus improving the geolocation accuracy of the scattering target.

3 GPS-R Link Budget for Target Detection

In order to understand whether or not the GPS backscattering from a target is detectable with respect to the background ocean clutter, we compute a realistic link budget, by simulating the received power for backscatter GPS from airborne scenarios, and we analyze it with respect to target size, receiver altitude, typical ocean backscatter at the GPS L-band, and typical noise floor of a GPS-R system.

3.1 Geometry

For simplicity, we assume here that transmitter, receiver and target are well aligned, so that the expression for the backscattered RCS from a corner reflector (easily available in literature) can be used. The geometry that we consider here is shown in figure 4.

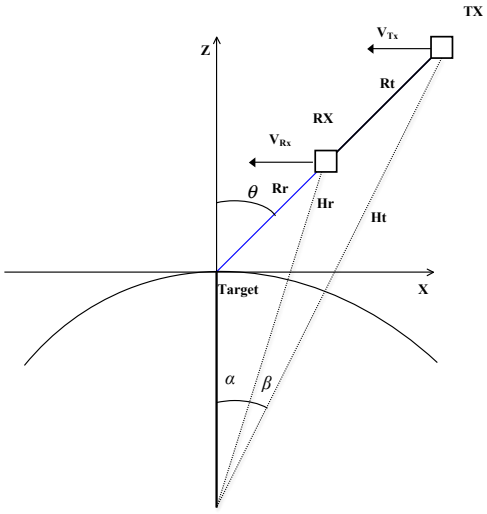

Figure 4. Geometry considered for this link budget. Transmitter and receiver have altitudes above the Earth of respectively H_r and H_t, and they have the same incidence angle θ.

We also assume a realistic GPS velocity vector of the transmitter, and we assume our receiver to be airborne and to travel in the direction opposite to where the transmitter is located (in other words, the x-component of the velocity vector of the receiver is negative if the transmitter position has positive x-component, or vice versa). The described geometry, and a sketch of how the iso-delay and iso-Doppler lines would approximately look, is shown in figure 5. Note that in a backscatter configuration the iso-delay lines are no longer ellipses centered on the target, but they tend to become parabolae, just like the iso-Doppler lines, hence the space-to-delay-Doppler mapping is similar to that found in a Synthetic Aperture Radar (SAR).

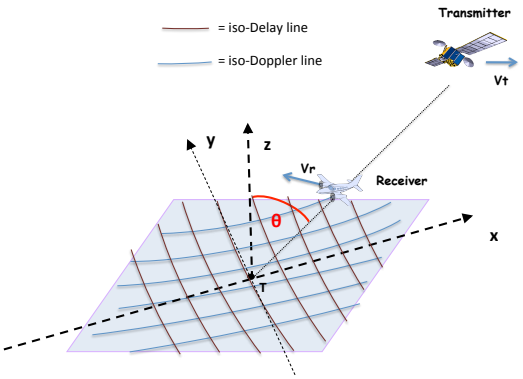

Figure 5. Geometry considered for these simulations, with transmitter and receiver lying in the *x*-*z* plane, both with positive *x*-component of their position, while the receiver velocity vector has negative *x*-component.

3.2 Target Backscattered Power

A general expression for the GPS received power from the ocean surface, as a function of delay t and Doppler frequency f, is given by [15]:

$$P_R(\tau,f)=\frac{P_T\lambda^2}{(4\pi)^3}\iint_A \frac{G_T(x,y)G_R(x,y)W^2(\tau,f;x,y)\sigma_0(x,y)}{R_T^2(x,y)R_R^2(x,y)}d^2r \quad (1.a)$$

$$W(\tau,f;x,y)=\Lambda^2(\tau;x,y)\left|S(f;x,y)\right|^2 \quad (1.b)$$

where

1) x and y are the coordinates of the generic scattering point in space, and τ and f are the delay and Doppler coordinates;
2) P_T is the transmit power, and λ is the signal wavelength;
3) R_T and R_R are, respectively, the distances from the scattering point on the surface to the transmitter and receiver;
4) G_T and G_R are the transmit and receive antenna gain patterns;
5) W is the so-called Woodward Ambiguity Function (WAF), made of the GPS triangular autocorrelation function Λ of the PRN code [8], and of the response of the Doppler filter S (modeled as a *sinc* function, as shown in [15]);
6) σ_0 is the bistatic Normalized Radar Cross Section (NRCS).

In general, the integration in eqn. (1) is performed over the entire region of the ocean surface where the diffuse scattering comes from, and the scattered power is a 2D function of the pair of coordinates (τ, f) representing points on the ocean surface. When considering the scattering from a corner reflector on a ship, the scattered power from the target becomes:

$$P_R(\tau_S,f_S)=\frac{P_T\lambda^2G_T(x_S,y_S)G_R(x_S,y_S)W^2(\tau_S,f_S;x_S,y_S)\sigma(x_S,y_S)}{(4\pi)^3R_T^2(x_S,y_S)R_R^2(x_S,y_S)} \quad (2)$$

where the suffix S represents the target, x_s and y_s are the spatial coordinates of the target, τ_s and f_s are the delay and Doppler coordinates of the target, and $\sigma(x_s,y_s)$ is the Radar Cross Section (RCS) of the target. The corner reflector we consider to model the target response is a trihedral square reflector. Assuming that the transmitter and receiver are along the boresight direction of the reflector, we write the Geometrical Optics (GO) derived RCS as [16-17]:

$$\sigma(x_S,y_S)=\frac{12\pi l^4}{\lambda^2} \quad (3)$$

where l is the target interior edge dimension, and λ is the incident GPS wavelength (19 cm). In order to compute equation (3), we use the parameters listed in Table 1, and we analyze P_R for varying target dimension l.

Table 1. Parameters used for the simulation. The Receiver antenna gain at the target corresponds to the antenna peak value of the CYGNSS mission.

Parameter Name	Value
GPS Transmitted Power P_T	14.25 dBW
GPS Antenna Gain G_T	13 dBi
Receiver Antenna Gain G_R at the target	14 dBi
Incidence Angle θ	30°
GPS Altitude H_t	20200 km
Receiver Altitude H_r	1 km, 5 km and 20 km
GPS WAF $\Lambda^2()$ $\|S()\|^2$	1

3.3 Ocean Backscattered Power

In order to be able to detect a target, the target backscattered power must be stronger than both the receiver noise floor, and the estimated backscattered power from the ocean at L-band, for a given scattering area. The ocean backscattered power has been calculated using equation (4):

$$P_R(\tau_{SP},f_{SP})=\frac{P_T\lambda^2G_T(x_{SP},y_{SP})G_R(x_{SP},y_{SP})W^2(\tau_{SP},f_{SP};x_{SP},y_{SP})\sigma_0(x_{SP},y_{SP})A}{(4\pi)^3R_T^2(x_{SP},y_{SP})R_R^2(x_{SP},y_{SP})} \quad (4)$$

where *SP* stands for the generic point on the sea surface, A is the scattering area, and σ_0 is the backscattered NRCS at L-Band. Some examples of typical VV- and HH-backscattered NRCS at L-band can be found in [18]. For this study, we consider the two cases shown in figure 1 of [18] of typical low wind speed (5 m/s) and high wind speed (20 m/s), and for the first beam of the Aquarius L-Band scatterometer, since its incidence angle is ~30°, very close to the one assumed here (Table 1). We also assume a worst-case scenario by selecting the maxima NRCS

values, which occur at VV-polarization, for the two wind cases: these values are -10.5 dB for 5 m/s, and -6 dB for 20 m/s. Note that this is still an approximation, since the incident GPS signal is not linearly but circularly polarized. In order to derive the ocean backscattered RCS from the NRCS, we need to calculate the ocean scattering area *A*. Here we assume that our data are processed to form DDMs. This represents an easy processing scheme, traditionally adopted for ocean remote sensing. In this case, we can then approximate the scattering area as the area included within half the width of the GPS WAF along the delay and along the Doppler [14], that is within the ±0.5 chip delay interval, and within the ±0.5 Doppler interval. It is worth pointing out that other GPS-R data processing algorithms exist (i.e. SAR-type processing, see [19-20]), which are more complex, but deliver a better resolution (on the order of tens of meters) and consequently a smaller scattering area associated with the ocean backscatter.

The configuration of the iso-Delay and iso-Doppler lines for the DDM processing and the geometry described above is shown in figure 6. The intersection between the iso-delay lines at -0.5 chip and 0.5 chip, and the iso-Doppler lines at -0.5 kHz and 0.5 kHz is shown, and this area is approximately equal to 1.3 km^2 for receiver at 1 km altitude, 1.4 km^2 for receiver at 5 km altitude and 3 km^2 for receiver at 20 km altitude.

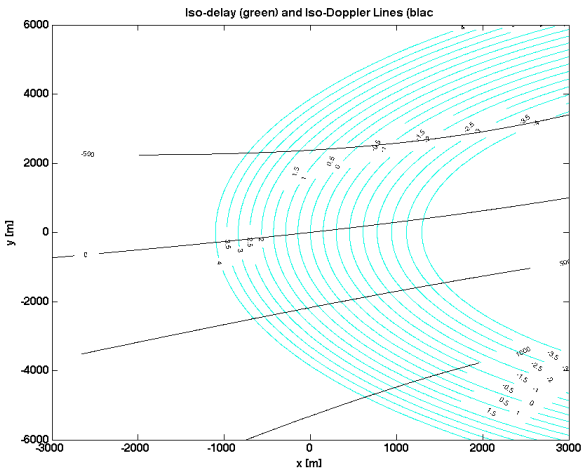

Figure 6. Configuration of iso-delay lines (green) over a 6 km x 12 km surface patch, with a GPS transmitter, and a receiver located at 5 km altitude. The iso-Doppler lines (black) are linked to the GPS and receiver velocity vectors, which have been described before. The spacing of the iso-delay lines is 0.5 chips, and the spacing of iso-Doppler lines is 500 Hz.

4 Simulation Results

Figure 7 shows the backscattered power from the target as continuous lines, as a function of target size, and for different altitudes of the receiver (blue: 1 km; cyan: 5 km and green: 20 km). The dashed and dotted-dashed lines represent respectively the backscattered power from the ocean at low wind (5 m/s), and at high wind (20 m/s), and they are reported for the three different receiver altitudes. Note that the backscattered power at high winds is always stronger than the backscattered power at low winds. The typical noise floor of a GPS-R system is shown in black.

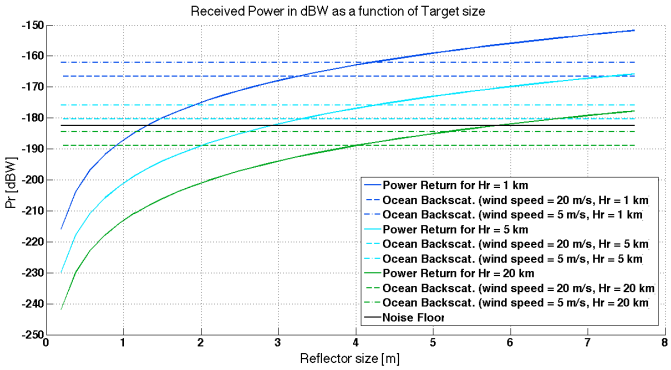

Figure 7. Plot of backscattered GPS Power P_R in dB, as a function of reflector size, for different receiver altitudes.

We can observe the following:

1) The P_R increases for increasing size of the corner reflector, and decreases for increasing receiver altitudes, as expected.

2) In order to observe a stronger return from the reflector compared to the ocean backscatter and the noise floor, we need a reflector size approximately > 4m for the two cases of 1 km and 5 km receiver altitude, and a reflector size > 6m for the 20 km receiver altitude case.

3) The target detection using GPS-R works better at lower altitudes, and over low wind regions. In these cases, the performances of the target detector are very similar at 1 km or 5 km altitude, and are mostly driven by the strength of the ocean backscatter compared to the target return.

The results in figure 7 have been obtained using conservative assumptions. For example, it might possible to reduce the ocean scattering area (which would bring down the ocean backscatter) by increasing the coherent integration time in the GPS processing, since the one used here is calibrated for spaceborne applications. A larger coherent integration times, which has been used in past airborne experiments [21], would reduce the size of the WAF along the Doppler, and hence the overall scattering area. The adoption of a different type of data processing algorithm, similar to that implemented in SAR [19-20], can also lead to a reduced ocean backscatter compared to the target. However, some additional effects like shadowing, fast-fading, or non-gaussian sea clutter can

easily contribute towards degradation of performances and therefore would need to be taken into account, when developing suitable detection algorithms. Finally, it is worth noting that a careful study on the optimal polarization of the receiver antenna should be performed, to enhance as much as possible the target backscattered signal with respect to the ocean clutter.

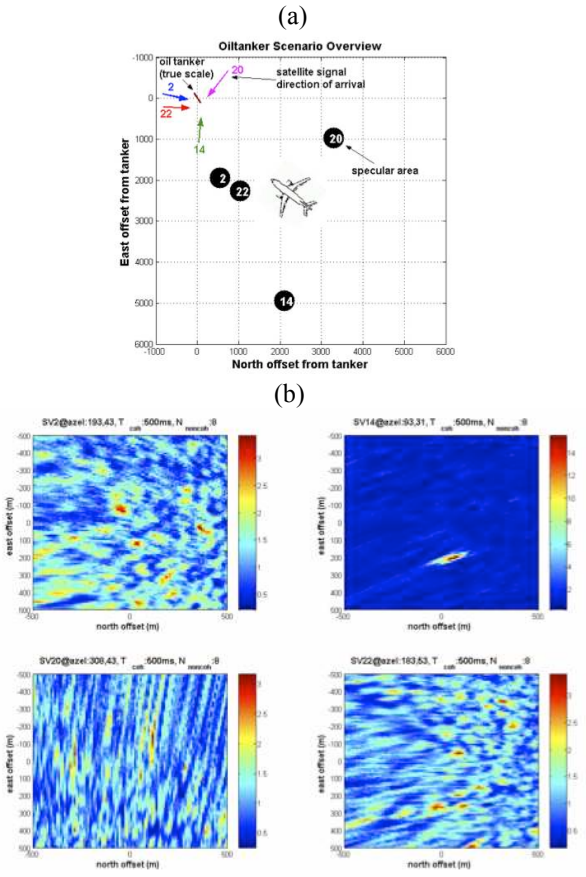

Figure 8 (from [22]): (a) scenario of the bistatic flight experiment described in [22]. The altitude of the airplane is 500 m. The four GPS satellites are identified by their PRN number (2, 14, 20 and 22). The colored arrows indicate the direction of arrival of the signal on the sea surface, and the black circles indicate the location of the specular point for each satellite. (b) Images of the scattered power from the sea surface for the four GPS signals (units of the color images are unknown). The signal in backscattering configuration from satellite PRN 14 is shown in the top right figure.

5 Literature Results Using Real Data

The novelty of the concept described in this paper is such that there is no direct experimental evidence of the detectability of targets using GPS-R. The only empirical evidence so far can be found in the work by *Brown et al.*, in [22], which shows, in an airborne experiment, that backscattered GPS signals can successfully detect targets (ships) over the ocean. To date, this is the only known study where a target was detected, and the detection attributed to the backscattering configuration of transmitter and receiver. The scenario of the experiment presented in [22] was made of a single target (an oil tanker) and of a GPS-R receiver onboard an airplane, simultaneously receiving reflected signals from four different GPS satellites, indexed by their unique Pseudo Random Noise (PRN) number. For convenience, we show here from [22] the flight experiment scenario in Figure 8a, along with the resulting signal returns from the different GPS PRNs, in Figure 8b.

PRN 14 was the only GPS transmitter positioned in a backscattering configuration among the four satellites in view. The reflections from each satellite were acquired through a high gain (+20 dBi) beam-steered antenna, and the reflections were processed to form a spatial image. Figure 8b shows that while none of the images obtained by satellites in forward scattering configuration show unequivocally the presence of the target, the image obtained by PRN 14, in a backscattering configuration, features a strong return from the oil tanker. Equally promising is the fact that the signal to clutter ratio for the PRN 14 measurement is significantly higher than the other cases (forward scatter cases), and that it is known that in this case the transmitter, target and receiver were not perfectly aligned, although the aspect angle was probably not too high.

6 Conclusions

In this paper, we have proposed a new approach to target detection, through the use of GPS signals of opportunity. We have computed a simplified link budget, assuming the perfect alignment of transmitter, target and receiver, which highlights that targets with corner reflectors larger than 4-6 m can be successfully detected at sufficiently low airborne altitudes, since their return is stronger than both the ocean clutter and the typical noise floor of GPS-R systems. This confirms the promising results shown in [22], which represents to-date the only empirical evidence of target detection using GPS-R.

The approach is very appealing due to the general advantages of GPS (or GNSS)-Reflectometry linked to the exploitation of pre-existing transmitters, the global coverage and high space-time sampling, and the use of simple, cheap, low-power and light-weight modified GPS receivers, that can be easily and naturally accommodated on a large number of platforms of different kind. For this application, it is suggested to use GPS backscattered signal, holding a number of advantages compared to the forward scattering configuration, among which the the sea clutter reduction, the "corner reflector" enhancement of the target return, and the elimination of spatial ambiguities. The results shown here are preliminary, but they give rise to a new exciting and convenient perspective for target detection. However, much more work is still needed to fully assess and characterize the validity of this approach. The most important steps we identify for work in the immediate future are: 1) the implementation of more

realistic simulations where transmitter, receiver and target are not aligned, to establish which range of geometries still allow to detect a target, and where the speckle component from the ocean backscatter is also included; 2) a study on what the optimal system parameters (i.e. coherent integration time, receiver antenna gain and noise figure etc.) and processing techniques (i.e. delay-Doppler processing, bistatic SAR-like processing etc.) would be for this application; 3) The identification of suitable detection algorithms for targets embedded in both Gaussian and non-gaussian/impulsive noise, and their characterization in terms of target size, geolocation accuracy and CFAR, and finally 4) The acquisition and analysis of some real data from airborne campaigns, to test and assess the identified processing techniques and detection algorithms.

References

[1] Marchan-Hernandez, J., Valencia, E., Rodriguez-Alvarez, N., Ramos-Perez, I., Bosch- Lluis, X., Camps, A., Eugenio, F., Marcello, J., "Sea-state determination using GNSS-R data," *IEEE Geoscience and Remote Sensing Letters* 7(4), 621–625, 2010.

[2] Clarizia, M.P., Ruf, C., Jales, P. and Gommenginger, C., "Spaceborne GNSS-R Minimum Variance Wind Speed Estimator". *IEEE Transactions on Geoscience and Remote Sensing* 52(11): 6829-6843, 2014.

[3] Rius, A., Cardellach, E. and Martín-Neira, M.,"Altimetric Analysis of the Sea-Surface GPS-Reflected Signals," *IEEE Transactions on Geoscience and Remote Sensing*, 48, 4, pp. 2119-2127, 2010.

[4] Gleason, S., Hodgart, S., Yiping, S., Gommenginger, C., Mackin, S., Adjrad and M., Unwin, "Detection and processing of bistatically reflected GPS signals from Low-Earth Orbit, for the purpose of ocean remote sensing," *IEEE Transactions on Geoscience and Remote Sensing* 43 (6), pp. 1229–1241, 2005.

[5] Clarizia, M., Gommenginger, Gleason, S., C., Srokosz, M., Galdi, C. and Di Bisceglie, M., "Analysis of GNSS-R delay-Doppler maps from the UK-DMC satellite over the ocean", *Geophysical Research Letters* 36, 2009.

[6] Misra P. and Enge P, *Global Positioning System: Signals, Measurements, and Performance*, Revised Second Edition, Ganga-Jamuna Press, 2011.

[7] Ruf, C., Lyons, A. and Ward, A., NASA Intensifies Hurricane Studies with CYGNSS," *The Earth Observer*, NASA, Vol. 25, Issue 3, 12-21, 2013.

[8] Ruf, C., Atlas, R., Chang P., Clarizia M.P., Garrison J., Gleason S., Katzberg, S., Jelenak Z., Johnson J., Majumdar S., O'Brien A., Posselt D., Ridley A., Rose R. and Zavorotny V., "New Ocean Winds Satellite Mission to Probe Hurricanes and Tropical Convection," *Bulletin of American Meteorological Society (BAMS)*, accepted for publication, 2015.

[9] Lu Y., Yang D., Li W., Ding J. and Li Z., "Study on the New Methods of Ship Object Detection Based on GNSS Reflection," *Marine Geodesy*, Vol. 32, Issue 1, 2013.

[10] Lindgren T., Vinande E. Akos D., Masters D. and Axelrad P. "Measurement of Backscattered GPS Signals," *Position, Location, And Navigation Symposium*, 2006 IEEE/ION, vol., no., pp.664,669, April 25-27, 2006.

[11] Kabakchiev C., Garvanov I., Behar V., and Rohling H., "The Experimental Study of Possibility for Radar Target Detection in FSR Using L1-Based Non-Cooperative Transmitter," *Radar Symposium* (IRS), 2013 14th International , vol.2, no., pp.625,630, 19-21 June 2013.

[12] Carrie, G., T. Deloues, J. Mametsa, S. Angelliaume, "Ship Detection Based on GNSS Reflected Signals: An Experimental Plan," *In proceedings of: Space Reflecto 2011*, At Calais, France.

[13] Soulat, F., Germain O., Fabry P., Hajduch G., Desjonqueres J.D. and Pourthie N., "Ship Detection Based on Airborne GNSS Reflections," *in Proceedings of the fourth Workshop on Advanced RF Sensors and Remote Sensing Instruments*, Noordwijk, Netherlands, 2014.

[14] Clarizia, M. P., "Investigating the effect of ocean waves on ocean-reflected GPS measurements," *PhD Thesis*, School of Ocean and Earth Sciences, University of Southampton, 2012.

[15] Zavorotny, V., Voronovich, A., "Scattering of GPS signals from the ocean with wind remote sensing applications," *IEEE Transactions on Geoscience and Remote Sensing* 38 (2), 951–964.

[16] Doerry A., "Reflectors for SAR Performance Testing", *SANDIA Report*, Jan. 2008

[17] Sarabandi K., and T. Chiu, "Optimum Corner Reflectors for Calibration of Imaging Radars", *IEEE Transactions on Antennas and Propagation*, vol 44, no. 10, Oct. 1996.

[18] Yueh, S.H., W. Tang; Fore, A.G.; Neumann, G.; Hayashi, A.; Freedman, A.; Chaubell, J.; Lagerloef, G.S.E., "L-Band Passive and Active Microwave Geophysical Model Functions of Ocean Surface Winds and Applications to Aquarius Retrieval," *IEEE Transactions on Geoscience and Remote Sensing,* vol.51, no.9, pp.4619,4632, Sept.2013.

[19] Ebinuma, T. and Mikawa Y., "Development of Bistatic GPS-SAR Image Processing Algorithm", *in Proceedings of the Symposium of Microsatellites for Remote Sensing (SOMIRES)*, Japan, 2013.

[20] M Cherniakov, R. Saini, R. Zuo, M. Antoniou, "Space-surface bistatic synthetic aperture radar with global navigation satellite system transmitter of opportunity-experimental results," *IET Proc. Radar Sonar Navigat*. 1(6), 447–458 (2007).

[21] Germain, O., Ruffini, G., Soulat, F., Caparrini, M., Chapron, B., Silvestrin, P., "The Eddy experiment: GNSS-R speculometry for directional sea-roughness retrieval from low altitude aircraft," *Geophysical Research Letters*, 31 (L12306), 2004.

[22] Brown A., and Mathews B., "Remote Sensing using Bistatic GPS and a Digital Beam 20 Steering Receiver," in *Proceedings of the ION GNSS*, 2005.